Iterative-SGLRT for Multiple Scatterers Detection in SAR Tomography

Hui Luo, Zhen Dong, Zhenhong Li, *Senior Member, IEEE*, and Anxi Yu

***Abstract*—This paper introduces a multiple scatterers detection method in synthetic aperture radar tomography (TomoSAR), named iterative sequential generalized likelihood ratio test (iterative-SGLRT). In this technique, the number of scatterers is sequentially decided by generalized likelihood ratio test (GLRT) pixel by pixel, after iteratively estimating the parameters. It is a good trade-off of the afore-proposed methods of sup-GLRT and fast-sup-GLRT on accuracy and efficiency. Simulated comparisons showed that iterative-SGLRT outperformed fast-sup-GLRT in the performances of detection probability and accuracy without substantial computation time increase, and compared to sup-GLRT, its performance loss could be negligible with computational burden greatly reduced. Additionally, both iterative-SGLRT and sup-GLRT have been applied to the TerraSAR-X dataset over Shenzhen city. 3D reconstruction of the test site and the separation of the overlaid scatterers have been achieved. Also, verification using light detection and radar (LiDAR) indicated an RMSE of $0.1\rho_s$ for both methods of the height estimated. Accordingly, iterative-SGLRT is very suitable for large urban area processing for its super-resolution, high efficiency, and robustness.**

***Index Terms*—Synthetic aperture radar tomography (TomoSAR); iterative sequential general likelihood ratio test (SGLRT); layover**

I. Introduction

AUTOMATIC detection and reconstruction of buildings and other man-made structures in urban areas are becoming increasingly important with the growth of metropolises. An extensive and ever-expanding archive of synthetic aperture radar (SAR) data, such as TerraSAR-X/TanDEM-X and COSMO-SkyMed, acquired over the last decade with higher resolution, has made it possible for considering the reconstruction and monitoring of urban infrastructures. Nevertheless, it also brings about the layover phenomenon, where multiple scatterers are mapped in the same range-azimuth resolution, especially for complex scenarios, such as high-rise buildings.

SAR tomography (TomoSAR), also known as 3-D SAR focusing technique, combines multibaseline (MB) acquisitions constituting a cross-track spatial array to fully image the scene in the 3-D space [1]–[3], i.e. to separate the overlaid targets. Beamforming (BF) [1] and singular value decomposition (SVD) [2], were firstly introduced to obtain the separation and location of such targets. However, the irregular baseline distribution results in a very sparse sampling pattern, which produces intolerable sidelobes or quasi-grating lobes in the estimated profiles. Worse still, the Rayleigh resolution, reciprocal to the perpendicular baseline extension, is often much poorer compared with horizontal resolution. The Capon method generally yields better performance than BF and SVD in terms of spatial resolution and leakage problems at the cost of reduced horizontal resolution [4]. Capon has also been extended to single-look data application after a sector interpolation, followed by the coherent averaging in the (uniform) spatial baseline domain [5]. Its performance, however, greatly depends on the so-called sector of interest (SOI), leading to big uncertainties [6]. Based on the fact that target distribution along elevation is always sparse, especially in urban areas, super-resolved compressed sensing (CS) provides another solution to deal with the TomoSAR inverse problem [7]–[9] . However, CS often implies a considerable computational burden, due to its iterative nature and due to the non-availability of the adapted efficient convex optimization algorithms.

In the case of multiple scatterers under study, the detection problem becomes hereafter. With constant false alarm rate (CFAR) characteristic, GLRT [9]–[11] has gained its popularity in recent years. The first attempts were carried out after BF imaging, achieving recognition of single scatterers [10], or obtaining robust detection of multiple scatterers [11]. To achieve super-resolution capabilities, sup-GLRT [13] has been proposed, at the cost of computational burden increase. The fast version of sup-GLRT, fast-sup-GLRT [14], [15], enjoys the computational efficiency as well a super-resolution capability comparable to that of sup-GLRT. However, as far as the accuracy concerned, its performance deteriorates especially in the super-resolution case.

To overcome the disadvantages of the above-mentioned methods, in the real-world TomoSAR operating scenarios, and with acceptable computational burden, a new multi-stage approach, named iterative sequential general likelihood ratio test (iterative-SGLRT), for TomoSAR imaging is proposed in this paper. It firstly iteratively estimates the parameters, followed by sequential GLRT test procedures until a model order is selected. Simulated results showed that it can achieve super-resolution, estimation accuracy and detection probability comparable to that of sup-GLRT with much less computation burden, and its accuracy has been greatly improved with acceptable computational burden increase compared with fast-sup-GLRT. In other words, iterative-SGLRT is a good trade-off for computational complexity and estimation accuracy.

This work was supported by National Natural Science Foundation of China (61771478).

H. Luo is with the college of electronic science of National University of Defense Technology, 410073 Changsha, China, and also with the School of Engineering, Newcastle University, NE1 7RU Newcastle, United Kingdom (email: luohui@nudt.edu.cn)

Z. Dong and Anxi Yu are with the College of Electronic Science, National University of Defense Technology, 410073 Changsha, China (e-mail: dongzhen@nudt.edu.cn, yu_anxi@nudt.edu.cn)

Z. Li is with the School of Engineering at Newcastle University, Newcastle NE1 7RU, United Kingdom, and also with the College of Geological Engineering and Geomatics, Chang'an University, 710054 Xi'an, China (email: zhenghong.li@newcastle.ac.uk)

Corresponding author: *Zhen Dong and Zhenhong Li*

Using TerraSAR-X dataset over Shenzhen city, China, the 3D urban reconstruction was obtained with an impressive density of 409,189 single scatterers and 26,843 double scatterers in an urban area of 0.8× 0.64 km^2,while those of sup-GLRT are 402,629 and 41,178, respectively. Verification using light detection and radar (LiDAR) indicated a root mean square error (RMSE) of $0.1\rho_s$ for both iterative-SGLRT and sup-GLRT of the height estimated, also validating the effectiveness of the proposed iterative-SGLRT method.

The novel contribution of this work relies mostly on the extension of the iterative estimation to the TomoSAR scenario, on the derivation of the generic parameter expression for this specific scenario, and on the propose of the efficient iterative-SGLRT with performances comparable to that of sup-GLRT. This paper is organized as follows. The theory basis is explained in Section II, and the processing flow of the proposed iterative-SGLRT is addressed in Section III. Section IV and V are devoted to the experiments on simulated and real data respectively. Finally, section V gives the conclusion.

II. Signal model and problem formulation

Considering a stack of N coregistered SLC images, in each pixel (x, r), the signal $\boldsymbol{g}$, after data calibration, i.e. the compensation of the phases coming from possible long-term scene deformations and atmospheric propagation effects, and appropriate discretizing operation, can be written as

$$\mathbf{g} = \mathbf{\Phi}\boldsymbol{\gamma} + \boldsymbol{\omega}, \tag{1}$$

where $\mathbf{\Phi}$ is the steering matrix, $\boldsymbol{\gamma}$ collects the samples of the backscattering distribution function, and $\boldsymbol{\omega}$ is the noise contribution. $\mathbf{\Phi}$ is dimensioned $N\times M$, whose generic element $(\boldsymbol{\phi}_i)_n$ is expressed as,

$$(\boldsymbol{\phi}_i)_n = \frac{1}{\sqrt{N}}\exp\{-j2\pi{\boldsymbol{\xi}_n}^T\mathbf{p}_i\}, \tag{2}$$

where ${\boldsymbol{\xi}_n}^T$collects the Fourier mate variables of the parameter vector $\mathbf{p}$, referred to as parameter vector, collects the parameters of interest (i.e., elevation for 3-D case; elevation and mean deformation velocity for 4-D case; and elevation, mean deformation velocity, and thermal dilation for the 5-D case). It spans the parameter space, which is discretized in M bins, corresponding to the parameter vectors $\mathbf{p}_1, ..., \mathbf{p}_M$. For the 3-D, 4-D, and 5-D cases, $\xi_n = [-\frac{2b_{\perp n}}{\lambda r}]$, $\boldsymbol{\xi}_n = [-\frac{2b_{\perp n}}{\lambda r}, 2t_n/\lambda]^T$, and $\boldsymbol{\xi}_n = [-\frac{2b_{\perp n}}{\lambda r}, 2t_n/\lambda, 2T_n/\lambda]^T$, respectively.

Considering the sparse characteristic, calibration error and possible noise in real scenario, we'd like to cast the problem under study a multiple hypothesis test as

$$H_k:\ \mathbf{g} = \sum_{i=1}^{k}\gamma_i\boldsymbol{\phi}(\mathbf{p}_i)\odot\mathbf{x}_i\odot\mathbf{e} + \boldsymbol{\omega}, k = 0, 1, ..., K. \tag{3}$$

H_k means the existence of k scatterers and K is the assumed maximum scatterers within a pixel. γ_i is the reflectively of the i^{th} scatterer, and the symbol $\odot$ denotes the Schur-Hadamard product. In addition, $\mathbf{x}_i$ is the multiplicative noise modeling the speckle vector, $\mathbf{e}$ contains possible residual random miscalibration error after atmospheric compensation [4].

III. Problem Solution

Firstly, a decoupling parametric estimation algorithm, termed as RELAX, is simply retrospected. It was proposed for the first time to estimate the sinusoidal parameters corrupted by autoregressive noise [16]. Referring to the signal model in Equation (3), it can also be regarded as a decoupling problem whose task is to estimate γ_i and $\mathbf{p}_i$. RELAX algorithm is a parametric technique, which solves recursively the NLS problem. It enjoys efficient computation, and accurate estimation. Interested readers can refer to [16] for details.

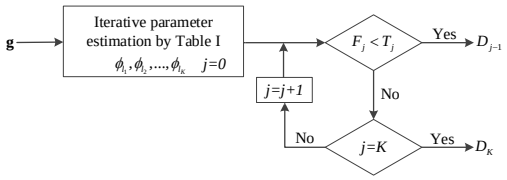

Fig. 1. Flow chart of the proposed iterative-SGLRT

Following the description in [14], fast-sup-GLRT can aggressively alleviate the computational burden in the original sup-GLRT method [13] by sequentially estimating the scatterer parameters. It is the approximated version of sup-GLRT and they are perfectly equivalent if the steering matrix is a square orthogonal one, i.e. with uniform baseline distribution and N=M. In realistic cases, these assumptions are often violated, thus leading to the performance loss both in accuracy and in detecting probability [14]. Therefore, a method with computational efficiency as well as with high accuracy is urgently in need.

Inspired by RELAX method, we propose an iterative-SGLRT method by introducing an iterative estimation procedure of the parameters to fast-sup-GLRT, whose procedures are depicted in Fig. 1. It adopts a two-step strategy to firstly iteratively obtain the related parameters, then to detect the number of scatterers sequentially by GLRT. Similar to the parameter estimation in RELAX, an iteratively sequential scatterer estimation is adopted here with details shown in Table I. Firstly, the multidimensional nonlinear minimization problem is transformed into a sequence of one-dimensional problems, with computation burden dramatically reduced. Then, the dominant component is estimated and its contribution is removed, then another component is estimated and its

TABLE I
Procedures for iterative estimation of scatterer parameters

Initializing,$\mathbf{\Phi}=\{\phi_1, \phi_2..., \phi_M\}$,$\widehat{\mathbf{\Phi}}_{\Omega_0}=\emptyset$,$C_1 = C_2 = 0$,$T\delta$, D
for $k = 1$ *to* K
$\mathbf{\Sigma}_{\mathrm{k}}=\mathbf{\Phi}-\widehat{\mathbf{\Phi}}_{\Omega_{k-1}}$,$\phi_{l_k}\in\mathbf{\Sigma}_k$, $\widehat{\mathbf{\Phi}}_{\Omega_k} = \left[\widehat{\mathbf{\Phi}}_{\Omega_{k-1}}, \phi_{l_k}\right]$
$\widehat{\mathbf{P}}_k^{\perp} = I_N - \widehat{\mathbf{\Phi}}_{\Omega_t}(\widehat{\mathbf{\Phi}}_{\Omega_k}^H\widehat{\mathbf{\Phi}}_{\Omega_k})^{-1}\widehat{\mathbf{\Phi}}_{\Omega_k}^H$, $\widehat{\phi}_{l_k} = \min_{\phi_{l_k}}|\mathbf{g}^H\mathbf{P}_k^{\perp}\mathbf{g}|$
$C_1 = \left|\mathbf{g}^H\widehat{\mathbf{P}}_k^{\perp}\mathbf{g}\right|$,$iter = 0$
while ($|C_1 - C_2| > T\delta$)& ($iter < D$)
$C_2 = C_1$, $iter = iter + 1$
for $j = 1$ *to* k
$\widehat{\mathbf{\Phi}}_{\Omega_{k-1}} = \left[\phi_{l_1}, ..., \phi_{l_i}, ..., \phi_{l_k}\right]_{i\neq j}$, $\mathbf{\Sigma}_k=\mathbf{\Phi}-\widehat{\mathbf{\Phi}}_{\Omega_{k-1}}$
$\widehat{\mathbf{P}}_k^{\perp} = I_N - \widehat{\mathbf{\Phi}}_{\Omega_k}(\widehat{\mathbf{\Phi}}_{\Omega_k}^H\widehat{\mathbf{\Phi}}_{\Omega_k})^{-1}\widehat{\mathbf{\Phi}}_{\Omega_k}^H$
$\phi_{l_j}\in\mathbf{\Sigma}_k$, $\widehat{\phi}_{l_j} = \min_{\phi_{l_j}}|\mathbf{g}^H\mathbf{P}_k^{\perp}\mathbf{g}|$, $C_1 = \left|\mathbf{g}^H\widehat{\mathbf{P}}_k^{\perp}\mathbf{g}\right|$
end
end
$\widehat{\mathbf{\Phi}}_{\Omega_k} = \left[\widehat{\phi}_{l_1}, ..., \widehat{\phi}_{l_j}, ..., \widehat{\phi}_{l_k}\right]$, $\widehat{\gamma}_{\Omega_k} = (\widehat{\mathbf{\Phi}}_{\Omega_k}^H\widehat{\mathbf{\Phi}}_{\Omega_k})^{-1}\widehat{\mathbf{\Phi}}_{\Omega_k}^H\mathbf{g}$
end

contribution is removed, and the previous estimate is refined. This procedure is repeated for each component to be estimated. The components are estimated recursively until a condition of convergence is satisfied. It appears that the specific sequence of steps pushes the search toward the global minimum of the NLS criterion. As the error introduced by the implementation of the minimization in a multi-dimensional space by means of sequential one-dimensional minimizations can be reduced by the iterative estimation procedure, iterative-SGLRT enjoys more accurate estimation than that of fast-sup-GLRT, though the computation burden is increased to a certain extent.

If we'd like to estimate the parameters of the k^{th} scatterer,

$$\widehat{\phi}_{l_k} = \min_{\phi_{l_k}} \left| \mathbf{g}^H \widehat{\mathbf{P}}_k^{\perp} \mathbf{g} \right|, \tag{4}$$

where $\widehat{\mathbf{P}}_k^{\perp}$ is projector onto the orthogonal complement to the subspace spanned by $\widehat{\mathbf{\Phi}}_{\Omega_k}$ with

$$\widehat{\mathbf{P}}_k^{\perp} = I_N - \widehat{\mathbf{\Phi}}_{\Omega_k} (\widehat{\mathbf{\Phi}}_{\Omega_k}^H \widehat{\mathbf{\Phi}}_{\Omega_k})^{-1} \widehat{\mathbf{\Phi}}_{\Omega_k}^H. \tag{5}$$

It is worth noting that $\widehat{\mathbf{\Phi}}_{\Omega_k} = [\widehat{\mathbf{\Phi}}_{\Omega_{k-1}}, \phi_{l_k}]$ and $\phi_{l_k} \in \mathbf{\Sigma}_k$ with $\mathbf{\Sigma}_k$ being complemented with $\widehat{\mathbf{\Phi}}_{\Omega_k - 1}$, i.e. $\mathbf{\Sigma}_k = \mathbf{\Phi} - \widehat{\mathbf{\Phi}}_{\Omega_k - 1}$. Then the parameters of the $1^{st} \sim (k-1)^{th}$ scatterers are re-estimated sequentially. When estimating the parameters of a specific scatterer, those of the others are set as known. With respect to the j^{th} scatterer, $\widehat{\mathbf{\Phi}}_{\Omega_{k-1}} = [\phi_{l_1}, ..., \phi_{l_i}, ...\phi_{l_k}]$, $i \neq j$. $\mathbf{\Sigma}_k = \mathbf{\Phi} - \widehat{\mathbf{\Phi}}_{\Omega_k - 1}$, $\phi_{l_j} \in \mathbf{\Sigma}_k$. Then, ϕ_{l_j} is computed by Equations (5) and (4). The estimation terminates when the cost function difference between two successive iterations becomes smaller than a certain threshold (with a typical value of $T\delta = 10^{-3}$).

After the parameter estimation, the detecting problem is solved by exploiting the strategy that adopted in sup-GLRT,

$$F_i(\mathbf{g}) = \frac{\left| \mathbf{g}^H \tilde{\mathbf{P}}_{i-1}^{\perp} \mathbf{g} \right|}{\min\limits_{j,\ j=i,...,K} \left| \mathbf{g}^H \tilde{\mathbf{P}}_{j}^{\perp} \mathbf{g} \right|} \underset{D_{i-1}}{\overset{D_{k \geq i}}{\gtrless}} T_i. \tag{6}$$

$F_i(\mathbf{g})$ measures the residual ratio of the hypothesis of H_{i-1} and $H_{k \geq i}$. Please note that although RELAX does not provide ML estimation and Equation (6) is no longer a likelihood ratio, we still call it SGLRT for its similar expression structure to that of sup-GLRT. As far as the thresholds T_i involved in each step i, they can be derived following a CFAR approach, consisting in setting T_i in such a way to obtain at each step i an assigned probability of false detection P_{fd_i} (one can refer to the definition in [13]). If not specifically clarified, $P_{fd_i} = 10^{-3}$ is fixed. All the thresholds can be numerically evaluated by means of Monte Carlo simulation. To be noted that, $\mathbf{p_i}$ corresponds to the positions of ϕ_i, $i = 1, 2, ..., k$.

IV. Experiments on Simulated Data

This section is devoted to the experimental results on simulated data, specifically to the comparisons on performances, e.g. computation burden, detection probability, and estimation accuracy, among iterative-SGLRT, sup-GLRT and fast-GLRT. For simplicity, only 3D case is considered here, i.e. parameters related to elevation s, if not specifically declared.

Theoretically, the computational complexities of iterative-SGLRT, sup-GLRT and fast-sup-GLRT are $\frac{K(2M-K+1)}{2} \sum_{k=2}^{K} kN_k(M-k+1)$, C_M^K, and $\frac{K(2M-K+1)}{2}$, respectively. M is the sampling rate, N_k is the iteration number used for the estimation of the k^{th} scatterer in iterative-SGLRT, and C_M^K means the combination number, i.e. the number of ways of picking K unordered outcomes from M possibilities, with the formula expressed as $C_M^K = \frac{M!}{K!(M-K)!}$, where $(*)!$ is a fractional.

Let β_i and β_s the ratio of computational complexity of iterative-SGLRT and sup-GLRT over that of fast-sup-GLRT respectively, then $\beta_{i(K=2)} \approx 10$, $\beta_{s(K=2)} \approx 20$ and $\beta_{i(K=3)} \approx 25$, $\beta_{s(K=3)} \approx 500$ (M and N_k are assumed 100 and 5 here, respectively). The computational time has been measured in testing the influence of the predefined maximum scatterers K and of the sampling rate M under $\Delta s = \rho_s$ (Δs means scatterer separation distance) , as shown in Fig. 2. In the left figure, the results have been obtained by averaging 100 trials with $M = 100$, while those in the right figure are deprived by averaging 1000 trials with $K = 2$. Generally speaking, sup-GLRT (green, triangle) is the most time-consuming among the 3 methods, especially with when $K > 2$, although the computational time of iterative-sup-GLRT (red, square) is consistently higher than that of fast-sup-GLRT (blue, dotted). A quasi-linear increase of computational time of K is apparent for iterative-SGLRT and fast-sup-GLRT, while that for sup-GLRT is much quicker. Under different M, it shows the same linear trend for fast-sup-GLRT and for iterative-SGLRT, and a combinatorial one for sup-GLRT.

Then, the detection probability (P_{di}) versus signal-to-noise ratio (SNR) and Δs is inspected, as shown in Fig. 3. Note that the discretization step for the experiments is fixed as $\rho_s/30$ and the scatterers are on-grid positioned. In the left figure, the two

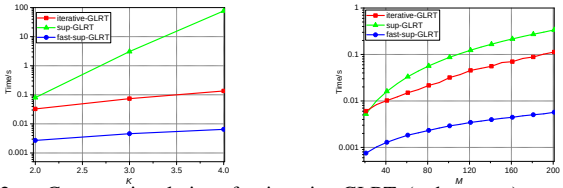

Fig. 2. Computational time for iterative-GLRT (red, square), sup-GLRT (green, triangle) and fast-sup-GLRT (blue, circle) versus the size of the predefined maximum scatterer K ($M = 100$) (left) and of the sampling number along elevation M ($K = 2$) (right).

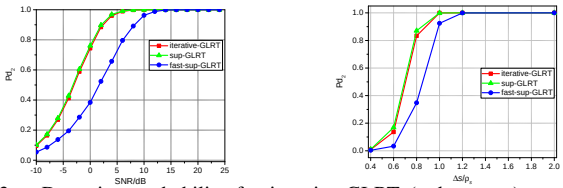

Fig. 3. Detection probability for iterative-GLRT (red, square), sup-GLRT (green, triangle) and fast-sup-GLRT (blue, circle) versus SNR (left) and scatterer separation (normalized to ρ_s) (right).

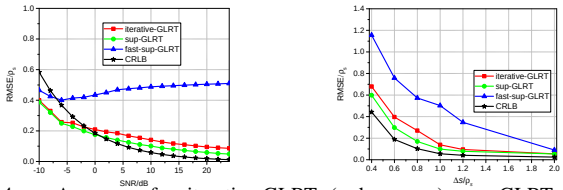

Fig. 4. Accuracy for iterative-GLRT (red, square), sup-GLRT (green, triangle), fast-sup-GLRT (blue, circle) and CRLB (black, star) versus SNR (left) and scatterer separation (normalized to ρ_s) (right).

scatterers are positioned with $\Delta_s = \rho_s$, with equal magnitude and with zero phase difference (in-phase). In the right figure, SNR is fixed (SNR$_1$=SNR$_2$=10dB). P_{d2} is computed under 10^4 Monte Carlo simulations with $P_{fd2} = 10^{-3}$. Under this specific condition, iterative-SGLRT enjoys almost the same detection probability with that of sup-GLRT, and outperforms that of fast-sup-GLRT, both under different SNRs and Δs.

As far as the accuracy concerned, RMSE of elevation is investigated. Note that, only the cases that the number of scatterers is correctly detected, i.e. (D_k/H_k), are considered for RMSE computing, and RMSE is defined as

$$RMSE_k = \sqrt{\frac{\sum_{p=1}^{N_k}\sum_{i=1}^{k}\left(\widehat{s}_{pi} - s_{pi}\right)^2 \Big/ k}{P_k}} \tag{7}$$

where s_{pi} and $\widehat{s}_{pi}$ are the true and estimated positions of the i^{th} scatterer of the p^{th} case with k scatterers, and P_k is the total number of the cases fulfil (D_k/H_k). As shown in Fig. 4, RMSE is plotted versus SNR (left) and versus Δs (right) under the same experimental conditions with that used in Fig. 3, respectively. Also, the theoretical limit of accuracy–Cramer Rao Low Bound (CRLB) [9], [12] is plotted for comparison. From the figures, we can see that the error increases with the decrease of SNR, as the difficulty in separating the signals from increased noise. In addition, the error increases as Δs decreases, especially in the super-resolution region, i.e., $\Delta s < \rho_s$, because of the difficulty in separating closely located scatterers. Iterative-SGLRT possesses negligible accuracy degradation with respect to that of sup-GLRT, which far outperforms that of fast-sup-GLRT, and approaches to CRLB. Note that, when SNR$<$0 dB, the accuracy performance of the algorithms seems superior to CRLB, which is probably an illusion resulted by the relative low detection probability under high noise level.

Some comments on the proposed iterative-SGLRT method are now in order. Firstly, it is more computationally efficient than that of sup-GLRT, as the iterative step always converges after several iterations (typical around 5 times). Secondly, its performances are comparable to that of sup-GLRT, which are superior to that of fast-sup-GLRT. Accordingly, It provides an alternative for sup-GLRT and fast-sup-GLRT to achieve good performances at acceptable computation burden. It can be perfectly used in the scatterers separation, especially in large scale urban area.

V. Experiments on real data

The iterative-SGLRT method, discussed in the previous section, has been applied to a real data stack formed by a total of 26 TerraSAR-X spotlight images (0.25m-resolution) over Shenzhen, China, acquired from January to December 2016 over descending passes. To process all the images, a referenced image, acquired on July 10, 2017, was selected while the others were all coregistered to it. The spatial and temporal baseline distributions are shown in Fig. 5, where the referenced one is labeled as a five star and the others are denoted as diamonds. The baseline distribution is highly non-uniform, with an overall perpendicular baseline of about 400m, resulting in an elevation resolution of about 28m (19.4m in height).

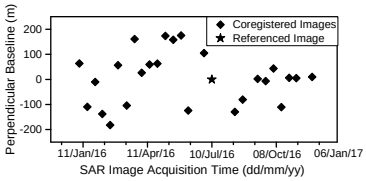

Fig. 5. Spatial/temporal baseline distribution.

We have selected, at full resolution, an area of 4800 pixels in azimuth (0.8 km) and 1400 pixels in range (0.64 km), [see the optical image from GoogleEarth and the incoherently averaged radar scene in Figs. 6(a) and (f) respectively]. In Fig. 6(f), the layover induced by the buildings is well recognized. Prior to the application of the detection algorithm, some preprocessing, e.g. phase calibration, has been performed. We suppose up to 2 scatterers (single and double) are overlaid in a range-azimuth cell.

In Fig. 6, we have compared the reconstructed topography deprived from the proposed iterative-SGLRT [(b)$\sim$(e)] with that from sup-GLRT [(g)$\sim$(j)]. By both methods, the density of the detected single scatterers is impressive with a total number of 409,189 for iterative-SGLRT [Fig. 6(b)], and 402,619 for sup-GLRT [Fig. 6(g)], respectively. The numbers of detected double scatterers [Figs. 6(c) and (h) for the higher layers, and (d) and (i) for the lower layers] are much less, with 26,843 for iterative-SGLRT and 41,178 for sup-GLRT. We can see that, the quantity and location of the detected scatterers are very similar, although the number of detected double scatterers of sup-GLRT is a little greater than that of iterative-SGLRT. This is mainly because that sup-GLRT is more tolerant to noise and composes a slight better super-resolution capability. So when the noise level is high or two scatterers are closely located, iterative-SGLRT can only detect single scatterers while sup-GLRT tends to detect as double scatterers. For sup-GLRT, among the detected double scatterers, 14,602 scatterers are with height differences smaller than $0.1\rho_s$, while that for iterative-GLRT is only 10.

Buildings rising toward the sensor is well recognizable in the detected scatterers. Nevertheless, some outliers are present mainly for two reasons. Firstly, a certain false alarm rate is allowed during the detection, in this case $P_{fa} = 10^{-3}$. Then, the existence of possible phase miscalibration may contribute to incorrect detection. Actually, the intrinsic processing difficulties of the starring spotlight data over other data stacks [17] are also outlier sources. Not surprisingly, most of the double scatterers are found around the buildings, showing the capability of iterative-SGLRT and sup-GLRT to separate the interfering layovers associated with the ground, the facade and/or the roof of the buildings.

Note that, in areas around the stadium [the area red-squared in Fig. 6(f)], it is difficult to quantify the height difference between the higher and lower layers. For this reason, difference maps were also provided for better illustration [see Figs 6(e) and (j)]. Please also note that, the stadium top can be penetrated [18], leading to the sensor receiving signals from the top, the chairs with different topography and the ground. So the detected higher layer can be from the stadium top and/or

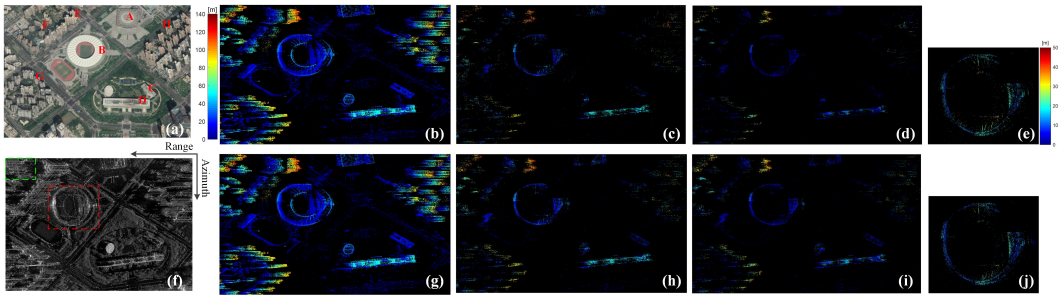

Fig. 6. Experiments on real data. Image of the area under study (a) Image@GoogleEarth and (f) SAR image. Reconstructed topography by iterative-SGLRT (b)∼ (e) and sup-GLRT (g)∼ (j) with (b) and (g) single scatterers, (c) and (h) higher layer of double scatterers , (d) and (i) lower layer of double scatterers, and (e) and (j) the height difference between the higher and lower layers of the area red-squared in (f). (c),(d) and (g)∼ (i) share the same colorbar with (b), while (e) and (j) share the other colorbar.

TABLE II
COMPARISON BETWEEN THE ESTIMATED HEIGHTS BY ITERATIVE-SGLRT/SUP-GLRT AND LIDAR (UNIT: M)

Method	A	B	C	D	E	F	G	H	RMSE
$iterative-SGLRT$	34.6	43.2	27.0	54.6	128.8	74.5	97.5	107.6	1.9
$sup-GLRT$	34.6	43.2	27.0	54.5	128.8	74.5	97.7	107.6	1.9
$LiDAR$	34.2	41.0	26.2	51.2	125.6	74.2	98.1	108.7	–

the chairs, and the lower layer can be from chairs and/or the ground.

Also a small area with 130,763 candidate pixels (refer to pixels with magnitude greater than a certain value) has been chosen for computation time comparison [see the area green-squared in Fig 6(f)]. The average time consumed for each processed pixel of iterative-SGLRT is 0.0045s, while that of sup-GLRT is 0.119s, which again validates the time efficiency property of iterative-SGLRT. To test the estimation accuracy, some points on the buildings top (pointed out in Fig. 6(a)) were selected for quantitative analysis. The comparative results obtained by LiDAR are reported in Table II, which shows an RMSE of 1.9m ($\approx 0.1\rho_s$) for both iterative-SGLRT and sup-GLRT, which indicates the comparable estimation accuracy of iterative-SGLRT to that of sup-GLRT.

VI. CONCLUSION

A multiple scatterers detection method in SAR tomography has been proposed in this paper. It adopts an iterative parameter estimation method, which provides a good trade-off between sup-GLRT and fast-sup-GLRT on performances of estimation accuracy and computational burden. It greatly attenuates the computation complexity in sup-GLRT by transforming the multiple-dimensional problem into a multiple 1D ones, and achieves negligible performances degradation compared with that of sup-GLRT, which far outperforms that of fast-sup-GLRT. Note that iterative-SGLRT is originally designed for urban areas, but actually it is perfectly applicable to other layover areas, which are characterized by the presence of a steep enough surface topography, generating critical projection of the scatterers in the slant imaging geometry.

REFERENCES

[1] A. Reigber, and A. Moreira, "First Demonstration of Airborne SAR Tomography Using Multibaseline L-Band Data," *IEEE Trans. Geosci. Remote Sens.*, vol. 38, no. 5, pp. 2142–2152, Sep. 2000.

[2] G. Fornaro, F. Serafino, and F. Soldovieri, "Three-Dimensional Focusing With Multipass SAR Data," *IEEE Trans. Geosci. Remote Sens.*, vol. 41, no. 3, pp. 507–517, Mar. 2003.

[3] X.X. Zhu, A.X. Yu, Z. Dong, M.Q. Wu, D.X. Li, and Y.S. Zhang, "New approach for robust and efficient detection of persistent scatterers in SAR tomography.", *Remote Sens.*, vol. 11, pp. 356, 2019.

[4] F. Lombardini, and M. Pardini, "Superresolution differential tomography: Experiments on identification of multiple scatterers in spaceborne SAR data," *IEEE Trans. Geosci. Remote Sens.*, vol. 50, no. 4, pp. 1117–1129, Apr. 2012.

[5] F. Lombardini, F. Cai, and D. Pasculli, "Spaceborne 3-D SAR Tomography for Analyzing Garbled Urban Scenarios: Single-Look Superresolution Advances and Experiments," *IEEE J. Sel. Top. Appl. Earth Observ. Remote Sens.*, vol. 6, no. 2, pp. 960–968, Apr. 2013.

[6] F. Lombardini, and M. Pardini, "3D SAR tomography: The multibaseline Sector Interpolation Approach," *IEEE Geosci. Remote Sens. Lett.*, vol. 5, no. 4, pp. 630–634, Oct. 2008.

[7] A. Budillon, A. Evangelista, and G. Schirinzi, "Three-dimensional SAR focusing from multipass signal using compressive sampling," *IEEE Trans. Geosc. Remote Sens.*, vol. 49, no. 1, pp. 488–499, Feb. 2011.

[8] X.X. Zhu, and R. Bamler, "Tomographic SAR Inversion by L1-Norm Regularization- The Compressive Sensing Approach," *IEEE Trans. Geosci. Remote Sens.*, vol. 48, no. 10, pp. 3839–3846. Oct. 2010.

[9] H. Luo, Z.H. Li, Z. Dong, A.X. Yu, Y.S. Zhang and X.X. Zhu, "Super-resolved Multiple Scatterers Detection in SAR Tomography Based on Compressive Sensing Generalized Likelihood Ratio Test (CS-GLRT)," *Remote Sens.*, vol. 11, pp. 1930, 2019.

[10] A. De Maio, G. Fornaro, and A. Pauciullo, "Detection of Single Scatterers in Multidimensional SAR Imaging," *IEEE Trans. Geosci. Remote Sens.*, vol. 47, no. 7, pp. 2284–2297, July 2009.

[11] A. Pauciullo, R. Diego, A. De Maio, and G. Fornaro, "Detection of Double Scatterers in SAR Tomography," *IEEE Trans. Geosci. Remote Sens.*, vol. 50, no. 9, pp. 3567–3586, Sept. 2012.

[12] X.X. Zhu, and R. Bamler, "Super-Resolution Power and Robustness of Compressive Sensing for Spectral Estimation With Application to Spaceborne Tomographic SAR," *IEEE Trans. Geosci. Remote Sens.*, vol. 50, no. 1, pp. 247–258. Jan. 2012.

[13] A. Budillon, G. Schirinzi, "GLRT Based on Support Estimation for Multiple Scatterers Detection in SAR Tomography," *IEEE J. Sel. Top. Appl. Earth Observ. Remote Sens.*, vol. 9, no. 3, pp. 1086–1094, Mar. 2016.

[14] A. Budillon, A. C. Johnsy, and G. Schirinzi, "A Fast Support Detector for Superresolution Localization of Multiple Scatterers in SAR Tomography," *IEEE J. Sel. Top. Appl. Earth Observ. Remote Sens.*, vol. 10, no. 6, pp. 2768–2779, Feb. 2017.

[15] A. Budillon, A. C. Johnsy, and G. Schirinzi, "Extension of a fast GLRT algorithm to 5D SAR tomography of Urban areas," *Remote Sens.*, vol. 9, no. 8, pp. 844, 2017.

[16] J. Li, and P. Stoica, "Efficient Mixed-Spectrum Estiamtion with Applications to Target Feature Extraction," *IEEE Trans. Signal Proc.*, vol. 44, no. 2, pp. 281–195, Feb. 1996.

[17] N. Ge, F.R. Gonzalez, Y. Wang, Y. Shi, and X.X. Zhu, "Spaceborne Staring Spotlight SAR Tomography - A First Demonstration with TerraSAR-X," *IEEE J. Sel. Top. Appl. Earth Observ. Remote Sens.*, vol. 11, no.10, pp. 3743–3756, Oct. 2018.

[18] H. Luo, Z. Li, Z. Dong, P. Liu, C. Wang and J. Song, "A New Baseline Linear Combination Algorithm for Generating Urban Digital Elevation Models With Multitemporal InSAR Observations," *IEEE Trans. Geosci. Remote Sens.*, to be published, doi: 10.1109/TGRS.2019.2943919.